Journal of the Brazilian Society of Mechanical Sciences and Engineering (2019) 41:449
https://doi.org/10.1007/s40430-019-1955-9

TECHNICAL PAPER

Application of reliability-based robust optimization in spacecraft attitude control with PWPF modulator under uncertainties

Vahid Bohlouri[1,2] · **Seyed Hamid Jalali-Naini**[1]

Received: 11 December 2018 / Accepted: 12 September 2019 / Published online: 21 September 2019

Abstract
The main objective of this paper is to enhance the robustness of an on–off attitude control under uncertainties while limiting the probability of failure in attitude control. To do this, the concept of system optimization is utilized for detailed engineering of spacecraft control using reliability-based robust design optimization (RBRDO). The probability of failure of the attitude control is chosen by the system designer as the input of the RBRDO algorithm. The single-axis spacecraft attitude is controlled using a combination of the observer-based anti-windup modified PI-D with pulse-width pulse-frequency modulator in the presence of external disturbance. The on–off thruster is modeled with a delay followed by a second-order transfer function. The input frequency of the thruster is limited to 50 Hz. The uncertain parameters are given as the spacecraft moment of inertia, thrust level, and thruster delay. The controller gains are determined by using traditional, robust, and reliability-based robust design optimizations under uncertainties and disturbance. The simulations are carried out using quasi-normalized equations, along with reducing problem variables and computational burden, to obtain more applicable results for a preliminary design. The traditional optimization gives the highest pointing accuracy without uncertainty, whereas the robust optimization obtains an approximately flat behavior for the mean of absolute pointing error under uncertainties. Under this situation, RBRDO could satisfy the prescribed reliability with a small loss in accuracy for the on–off attitude control of spacecraft, but under system limitations.

Keywords Satellite attitude control · Reliability-based robust design optimization · On–off thruster · Uncertainty

1 Introduction

Spacecraft optimization algorithms are widely used and improved in many fields, especially in engineering to reduce the cost of design and/or to enhance the performance. These algorithms are increasingly utilized to enhance the performance of dynamical systems. In solving and optimization problem, an extremum point is obtained; however, the system performance reduces from a suboptimal and/or unreliable design to even an unstable behavior under uncertainties. For such situations, uncertainty-based optimization methods are suggested. Robust design optimization (RDO) algorithms have been developed to increase the robustness of systems under uncertainties. To ensure a level of safety, reliability-based design optimization (RBDO) has been introduced in order to achieve a prescribed probability of failure. This approach can also be utilized for subsystem design such as control systems [1, 2].

Most of the studies on uncertainty-based optimization deals with the system design such as a high-speed PM motor design [3], aerospace vehicles [4], and multidisciplinary system design for ship [5], satellite, and orbit design [6] using robust optimization. A benchmark study of numerical methods for RBDO is given in [7] describing mono-level RBDO approaches, two-level RBDO approaches, decoupled RBDO approaches; each of them consists of several methods.

The robust design optimization algorithm was first published by Taguchi in 1986 [8]; however, associated subjects such as sensitivity analysis, worst-case analysis, and

Technical Editor: Marcelo A. Trindade, Dr.

✉ Seyed Hamid Jalali-Naini
shjalalinaini@modares.ac.ir

Vahid Bohlouri
v_bohlouri@tvu.ac.ir

[1] Department of Mechanical Engineering, Tarbiat Modares University, P.O. Box 14115-111, Tehran, Iran

[2] Present Address: Technical and Vocational University, Mashhad, Iran

stochastic linear programming had been utilized before [1]. Mulvey presented the benefits of his RDO framework and compared it with stochastic linear programming in several examples [9].

In this context, several algorithms and frameworks introduced for RDO based on evolutionary algorithms such as genetic, simulated annealing, and tabu search algorithms [1, 10]. The classification of the RDO has been introduced and modified as described in details by [1]. The application of RDO on subsystem design is increasingly presented, especially in detailed engineering such as turbomachinery cascades [11], power capacity expansion [12], hybrid electric vehicles [13], and aerodynamic loadings for airfoil inverse design [14]. Also, robust design optimization is utilized in control of dynamical systems such as in [15–17]. In 2016, RDO was first utilized in control of satellite by Bruni and Celani. They obtained the controller gains for stabilization mode with magnetic actuators [18], on–off attitude control with observer-based PI-D using Schmitt trigger [19] and PWPF modulator [20], and recently, robust technique using an integration of global and local derivative-free optimization [21].

Under uncertainties and randomness of parameters, the design constraints are usually violated, especially in traditional optimization. Although RDO improve the robustness of the design with respect to traditional optimization, it does not guarantee the design reliability. The concept of RBDO is introduced, when the safety is ensured in uncertain parameters and models [1, 2]. The framework and algorithm of RBDO are presented and modified in [22–25].

In 1998, the combination of robust and reliable optimization was intended and utilized by Wang and Wue [26]. There are several frameworks which have presented by researchers to improve the reliability-based robust design optimization process. This concept is also utilized in crashworthiness design of vehicle structure [27] and water supply system [28]. There are several works on subsystem design utilizing RBDO [29–31] and in aerospace system design such as the design of a satellite constellation using collaborative optimization [32], conceptual remote sensing satellite design optimization [33], and multidisciplinary system design optimization of on-orbit satellite [8].

There are various control strategies for continuous and on–off spacecraft actuation systems. In robust control design with continuous actuation, which is beyond the scope of this work, two different methods have recently been utilized in [34, 35]. In on–off actuation systems, the modulators are developed in order to convert the continuous control signals to on–off signals. The pulse-width pulse-frequency (PWPF) modulator is common in on–off attitude control due to numerous advantages such as high precision, quasi-linear behavior, vibration reduction, and low fuel consumption [36]. Modulators are utilized in conjunction with other controllers such as proportional–integral–derivative (PID) and sliding mode [37]. The PID-type controllers are of high interest in practice, because of their simplicity, ease of use, and proper performance [38].

There are several PID modifications to improve the performance, namely conditional integration, proportional band and conditioning, back calculation, observer-based PID controllers, and hybrid algorithm [35, 38]. In the control literature, when the derivative is fed back, instead of a derivative in forward path, the controller is denoted by PI-D. The observer-based PID is an anti-windup modification, utilized in on–off satellite attitude control using PWPF modulator [39]. To reduce the total of design variables and computational burden, quasi-normalized equations are utilized as treated in [20].

The robust control design and stability analysis of spacecraft with on–off actuation system are complex because of the nonlinearity of the system as treated in [40]. The optimization techniques have opened an alternative approach to enhance the performance and robustness of nonlinear dynamical systems, especially for spacecraft attitude control. In this regard, RDO has recently been utilized in [18, 19] as mentioned earlier. A comparative study between RBDO and reliability-based robust design optimization (RBRDO) in an on–off satellite attitude control has been carried out for zero reference input [41]. To the authors' knowledge, the RBRDO in satellite attitude control has not been published in the open literature in order to limit the probability of the failure of the attitude control, which is the subject of the present work. Consequently, an observer-based anti-windup modified PI-D with PWPFM is utilized under several practical limitations.

2 On–off attitude control

On–off thruster actuators are used in satellite attitude control, especially when it comes to the need to generate high level of torque and fast response of control system. This type of actuator requires on–off controllers. A well-known PWPF modulator (PWPFM) is combined with classical controllers such as PD, PID, and PI-D or modern control algorithms such as LQR and sliding mode. In this study, an observer-based modified PI-D controller described in [20] is, here, utilized for satellite attitude control with on–off thruster actuators.

2.1 PWPFM + modified PI-D controller

The block diagram of a single-axis attitude control of a rigid satellite with on–off thruster is shown in Fig. 1 using PWPFM and observer-based modified PI-D controller [37]. In the block diagram, the angular position of the satellite (Θ)

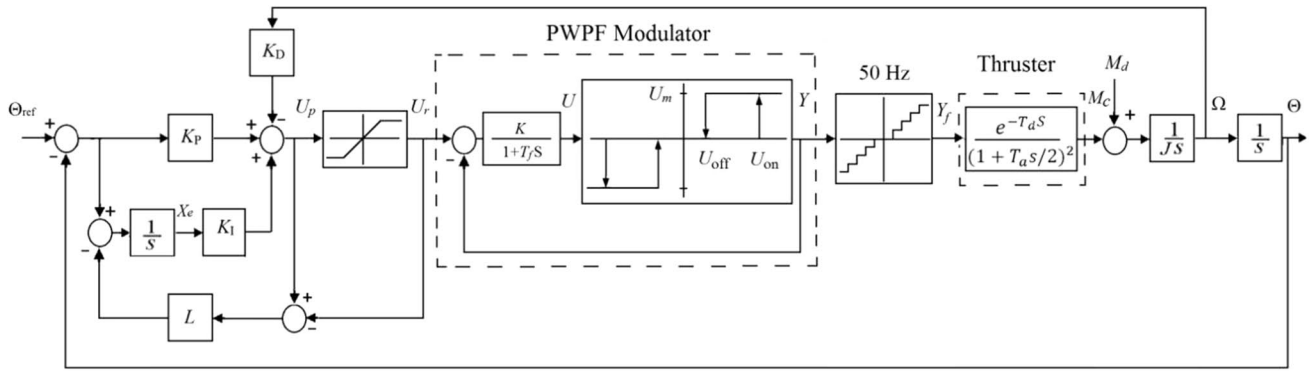

Fig. 1 Block diagram of a satellite attitude control with modified PI-D and PWPF modulator

is compared with the reference input (Θ_{ref}) and generates the error signal. This block diagram contains a modified PI-D, PWPF modulator, thruster model, satellite dynamic model, and feedback loops of attitude and its rate.

The anti-windup modified PI-D is used in order to reduce the steady-state error and to improve the performance of the attitude control. The modified PI-D controller benefits from an anti-windup circuit consisting saturation, integrator, a feedback loop, and observer gain as illustrated in Fig. 1. The PI-D gains and observer gain are denoted by (K_P, K_I, K_D) and L, respectively. Also, U_P and U_r are the respective saturation input and output. The PWPF modulator is shown with dashed-line box in the figure. The modulator consists of a low-pass filter with a filter gain of K and a time constant T_f, Schmitt trigger block, and a unity feedback. In the Schmitt trigger block, U_{on} and U_{off} are on and off thresholds, respectively, U_m is maximum torque of the modulator, and Y is the modulator output. The frequency of the input signal to the thruster, Y_f, is limited to 50 Hz due to practical considerations. The thruster actuator dynamics is taken as the second-order binomial transfer function with a time constant of T_a plus a delay of T_d. The external disturbance and control torque are denoted by M_d and M_c, respectively. The transfer function from input external torque to angular rate (Ω) of a single-axis rigid satellite is $1/J$s where s is the Laplace domain variable and J is the satellite moment of inertia.

2.2 Quasi-normalized equations

There are several design parameters for attitude control of a satellite as shown in Fig. 1. Using normalized or quasi-normalized forms of parameters reduces the number of system parameters. Consequently, the computational burden for optimization is reduced, and the obtained results are usable for a wide range of satellite specifications. An attitude control block diagram with quasi-normalized parameters is depicted in Fig. 2 using the following change of variables:

$$u = \frac{U}{KU_m}, u_{\text{on}} = \frac{U_{\text{on}}}{KU_m}, u_{\text{off}} = \frac{U_{\text{off}}}{KU_m}, u_{\text{old}} = \frac{U_{\text{old}}}{KU_m} \tag{1a}$$

$$u_p = \frac{U_p}{U_m}, u_r = \frac{U_r}{U_m}, u_{\max} = \frac{U_{\max}}{U_m}, u_{\min} = \frac{U_{\min}}{U_m} \tag{1b}$$

$$m_{\text{d}} = \frac{M_d}{U_m}, m_{\text{c}} = \frac{M_c}{U_m}, y = \frac{Y}{U_m} \tag{1c}$$

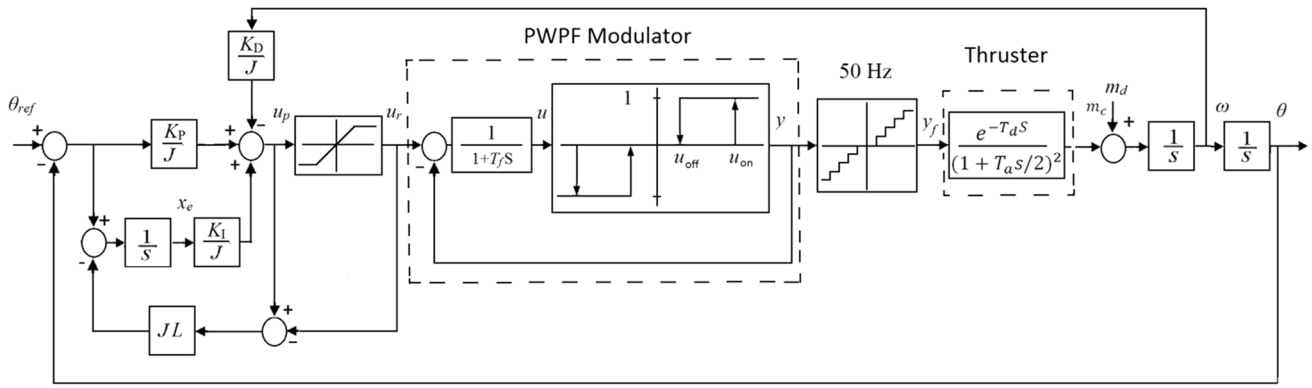

Fig. 2 Block diagram of a satellite attitude control using modified PI-D and PWPF modulator with quasi-normalized equations for U_m, K, J

$$\theta = \frac{J\Theta}{U_m}, \theta_{\text{ref}} = \frac{J\Theta_{\text{ref}}}{U_m}, \omega = \frac{J\Omega}{U_m}, x_{\text{e}} = \frac{JX_{\text{e}}}{U_m} \tag{1d}$$

$$k_p = \frac{K_p}{J}, k_D = \frac{K_D}{J}, k_I = \frac{K_I}{J}, l = JL \tag{1e}$$

The quasi-normalized state-space equations of the new system are given by

$$\dot{\theta} = \omega \tag{2a}$$

$$\dot{\omega} = m_c + m_d \tag{2b}$$

$$\dot{u} = \left[\left(u_r - y\right) - u\right]/T_f \tag{2c}$$

$$\dot{x}_e = \left(\theta_{\text{ref}} - \theta\right) - l\left\{\left[k_P\left(\theta_{\text{ref}} - \theta\right) + k_I x_e - k_D\omega\right] - u_r\right\} \tag{2d}$$

$$\dot{z}_1 = 2\left(y_d - z_1\right)/T_a \tag{2e}$$

$$\dot{z}_2 = 2\left(z_1 - z_2\right)/T_a \tag{2f}$$

where z_1 and z_2 are the state-space variables in the thruster model, x_e is the output of the integrator, and

$$y = f\left(u, u_{\text{on}}, u_{\text{off}}, u_{\text{old}}, 1\right) \tag{3}$$

$$y_d = y_f(t - T_d) \text{ for } t > T_d \tag{4}$$

$$u_r = \begin{cases} u_{\max} & \text{for } u_p \geq u_{\max} \\ u_p & \text{for } u_{\min} < u_p < u_{\max} \\ u_{\min} & \text{for } u_p \leq u_{\min} \end{cases} \tag{5}$$

in which $u_{\max}$ is the maximum value of the saturation block and $f(\cdot)$ is the functionality of the Schmitt trigger block. The control signal before and after saturation block is denoted u_p and u_r, respectively.

The second quasi-normalized form may be utilized when the satellite moment of inertia is specified. In this case, the parameters K and U_m are merged to other parameters as depicted in Fig. 3. Therefore, several normalized parameters are the same as in Eqs. (1a) to (1c), and the others are as follows:

$$\theta = \frac{\Theta}{U_m}, \theta_{\text{ref}} = \frac{\Theta_{\text{ref}}}{U_m}, \omega = \frac{\Omega}{U_m}, x_{\text{e}} = \frac{X_{\text{e}}}{U_m} \tag{6}$$

Table 1 The values of parameters in traditional optimization

Parameters	Value
u_{on}	0.045
$u_{\max}$	1
$u_{\min}$	−1
T_f	0.2 (s)
T_d	0.02 (s)
T_a	0.01 (s)

3 Traditional optimization

In the traditional optimization, the modified PI-D controller gains are determined using genetic algorithm. Our objective is the minimization of the time average value of the difference between the reference and actual angular position in a specified time interval at the end. A final error < 1% of the reference value and an overshoot < 10% are considered as our problem constraints. The optimization variables, that must be obtained, are k_P, k_D, k_I, l, and u_{off}. The algorithm will be stopped when the changes in objective function is less than 10^{-7}. In this formulation, the sensor noise can also be applied, but not considered here.

First, consider a single-axis attitude control with observer-based modified PI-D, according to Fig. 2, for rest-to-rest maneuvers. The values of fixed parameters in our optimization are listed in Table 1. The initial values of angular position and

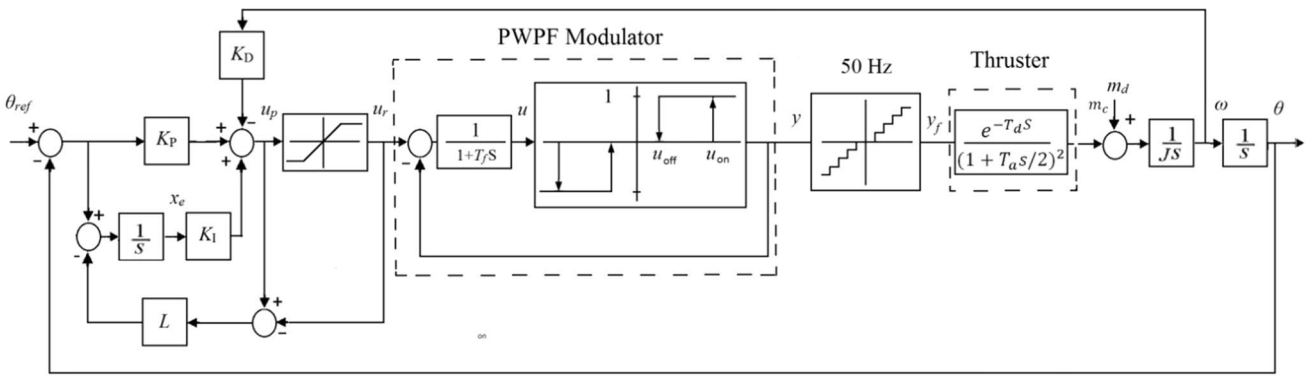

Fig. 3 Block diagram of a satellite attitude control using modified PI-D and PWPF modulator with quasi-normalized equations for U_m and K

Table 2 The values of controller gains

Θ_{ref} (deg)	K_P (N m/rad)	K_D (N m s/rad)	K_I (N m/rad)	L (rad/N m)	U_{off} (N m)
0	24.41	22.03	10.45	14.95	0.104
5	29.4	23.17	5.458	0.132	0.477
15	56.257	48.171	22.108	0.207	0.137
30	59.074	46.79	31.653	0.155	0.14
45	59.632	50.091	28.44	0.287	0.134
60	69.793	44.974	31.297	0.083	0.149
75	78.146	38.033	34.44	0.517	0.347

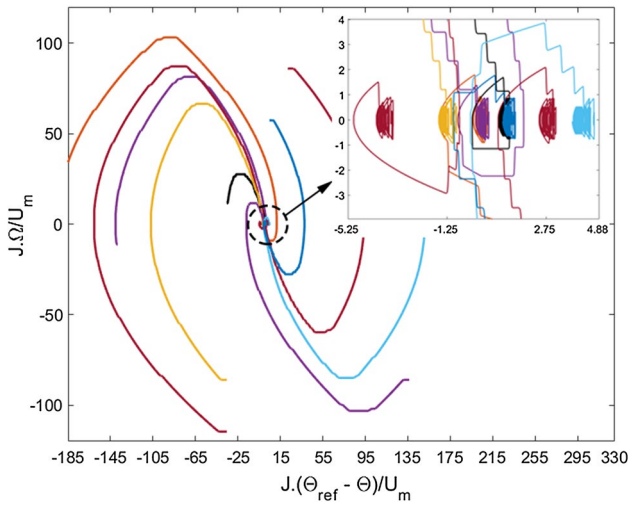

Fig. 4 Phase plane of the attitude control response for different initial conditions

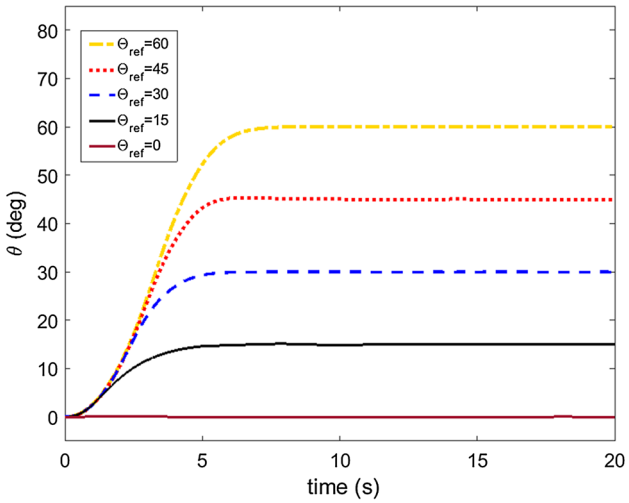

Fig. 5 Response of attitude control for different input angles

velocity are set to zero. The normalized external disturbance is given $m_d = 0.02$. Using genetic algorithm the problem variables are obtained, as shown in Table 2, for different values of $\theta_{\text{ref}} = 15, 30, 45, 60\,\text{s}^2$ deg. For this case, the objective is the minimization of the time average of the absolute pointing error. The absolute pointing error of the time average is restricted to 0.1 deg. To compute the objective function, a specified time interval of 20 s is chosen after an initial time interval of 10 s. For example, the behavior of the system with different initial values of angular position and velocity are shown in phase plane method for $\theta_{\text{ref}} = 15\,\text{s}^2$ deg in the presence of $m_d = 0.02$. The $\theta - \omega$ trajectory falls into a pseudo-limit cycle behavior as seen in the magnified part of Fig. 4.

To obtain a more quantitative sense, the optimization has also been carried out according to Fig. 1 for reference inputs of 0, 5, 15, 30, 45, and 60 deg. The values of parameters are set to be $T_d = 0.02\,\text{s}$, $T_a = 0.01\,\text{s}$, $T_f = 0.2\,\text{s}$, $J = 10\,\text{kg m}^2$, $U_m = 1\,\text{N m}$. The initial values of angular position and velocity are set to zero, and the external disturbance is $M_d = 0.02\,\text{N m}$. The results of optimization are given in Table 2 and utilized for robustness study of the control law. For this case, the attitude control response is shown in Fig. 5. The control response is chosen to be fast, because the objective function of the pointing error is computed after 10 s from rest. Depending on application, the control response can be chosen slower, as usual in most applications.

For the performance study of the optimized attitude control, at least $\pm 20\%$ uncertainties are considered for the moment of inertia, thruster level, external disturbance, and the actuator delay, according to Fig. 6. In this figure, the effects of the uncertainties on fuel consumption and thruster firings are plotted, separately for each uncertainty when the others are set to their nominal values. Fuel consumption is proportional to the integral of the absolute value of thruster output M_c, denoted by ΔV. For each reference input, the related determined parameters have been utilized according to Table 3. As expected, the graphs are symmetrical about $\Theta_{\text{ref}} = 0$. Although the depicted results show that the obtained parameters give an acceptable performance, it may not provide, in some situations, an acceptable performance due to uncertainties. In other words, the traditional optimization does not guarantee the performance of the system out of the nominal values of the optimized parameters. It seems there is a trade-off between the design based on low sensitivity due to uncertainties and increasing fuel consumption or thruster activities.

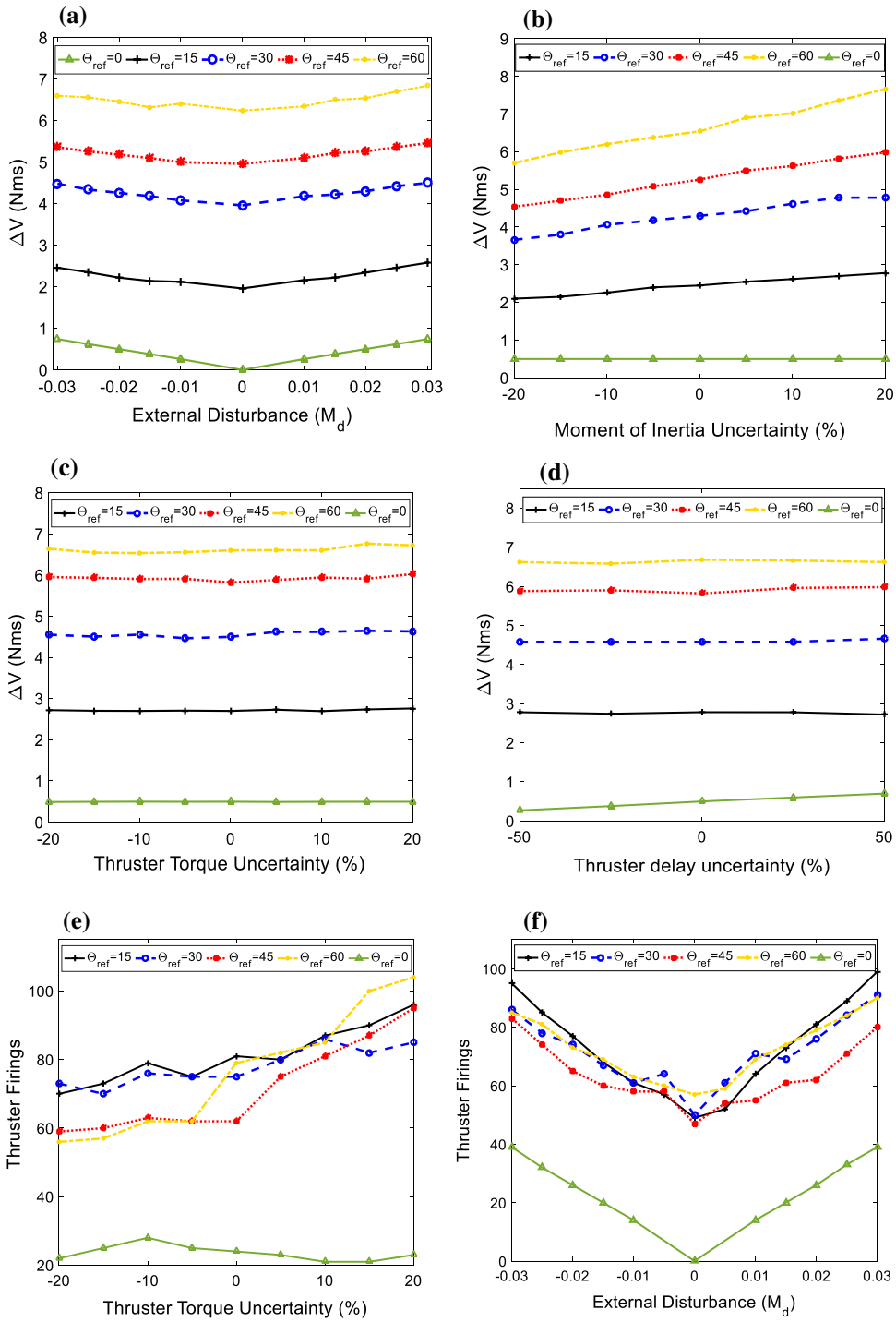

Fig. 6 Fuel consumptions and thruster firings versus uncertainties

Table 3 The values of the determined variables

Variable	Value
$k_P = K_P/J$	2.956 ($1/s^2$ rad)
$k_D = K_D/J$	2.757 ($1/s$ rad)
$k_I = K_I/J$	0.019 ($1/s^3$ rad)
$l = JL$	1.028 (s^2 rad)
$u_{\text{off}} = U_{\text{off}}/KU_m$	0.015

4 Robust optimization

The behavior of a typical attitude control system in the presence of uncertainties has been studied in Sect. 3. The performance of the system usually decreases in the presence of uncertainties. It may be unacceptable, and the

control response may violate the problem constraints due to uncertainties, even in a stabilized situation.

In robust optimization methodology based on evolutionary algorithm, statistical properties of uncertainties are considered in the optimization process as inputs of algorithms in order to increase the robustness of the system. A framework of reliability-based robust methodology, as illustrated in Fig. 7, including the following robust optimization statements, was presented in [33] as follows:

$$\begin{aligned}&\text{Find(y)}\\&\text{Minimizing } \phi(y,x) = P_E E\left[F(y,x)\right] + P_\sigma \sigma\left[F(y,x)\right] + \text{Penalty}(y,x)\\&\text{Subject to } \Gamma_i(y,x) = G_i(y,x) \le 0,\ i = 1,\dots I\\&y_j\text{min} \le y_j \le y_j\text{max}\end{aligned} \tag{7}$$

where y and x are the respective variable and parameter vectors of the optimization; F is the deterministic objective function; E and σ are the respective expected value and the standard deviation of F; and P_E and P_σ are constant weight coefficients of robust objective function ϕ, respectively. The Latin hypercube sampling (LHS) method is utilized to generate the Gaussian random variables as in [31]. The robust objective function includes a weighted combination of E and σ and a penalty function of Penalty(y,x). To decrease the computational burden in optimization, penalty function method is considered. According to Fig. 7, the penalty function takes a very large value, when the constraints are violated; otherwise, the penalty function is zero. The number of constraints is denoted by I and G_i is the ith constraint $(i = 1,\dots,I)$. In the robust optimization algorithm, the dashed-line box in Fig. 7 is omitted; therefore, Γ_i becomes equal to G_i in Eq. (7). The maximum and minimum range of variables in y construct the components of vectors $y_j$max and $y_j$min, respectively. The stopping criterion is $\phi < \varepsilon$ where ε takes a very small value.

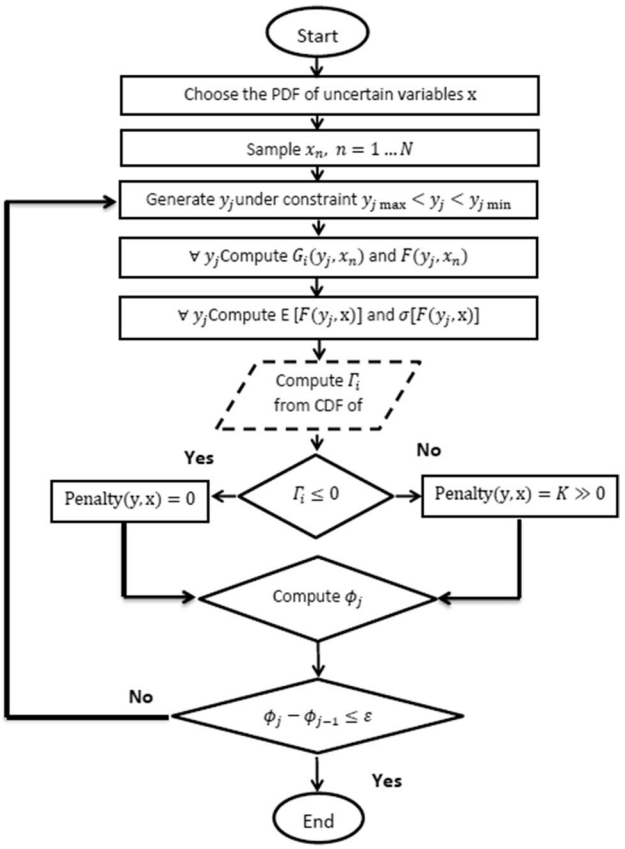

Fig. 7 Reliability-based robust optimization flowchart [31]

In order to apply the uncertainty of the moment of inertia, the quasi-normalized form, described in Fig. 3, is utilized as mentioned earlier. Here, the modified PI-D controller gains (K_P, K_D, K_I, L) of the quasi-normalized attitude control in Fig. 3 are obtained using the mentioned framework of the robust optimization in the presence of uncertainties. Uncertainties in thrust level, moment of inertia, thruster delay, and external disturbance take into consideration according to Table 4. A constant external disturbance is considered with an uncertainty, which has a different value for each run. The formulation of robust optimization (7) in the satellite attitude control, illustrated in Fig. 7, can be written as follows:

$$\begin{aligned}&\text{Find } \left(K_P, K_D, K_I, L\right)\\&\text{Minimizing } \phi(y,x) = P_E E[\bar{e}] + P_\sigma \sigma[\bar{e}] + \text{Penalty}(y,x)\\&\text{Subject to } G1 : (\text{Max}(|\text{Err}|) - 0.1) \le 0 \quad (I = 1)\\&0.1 \le K_P, K_D, K_I, L \le 200\end{aligned} \tag{8}$$

where (K_P, K_D, K_I, L) is variable vector y; (J, U_m, T_d, M_d) is parameter vector x; Err is the quasi-normalized pointing error; and

$$\bar{e} = \frac{1}{(t_f - 10)} \int_{10}^{t_f} |\text{Err}| \text{d}t \tag{9}$$

in which $t_f = 30$ s is the final time of the numerical simulation. The time average of the absolute value of the quasi-normalized pointing error, $\bar{e}$, is considered as the original (traditional) objective function (F), computed after 10 s to the final time. The problem constraint is the maximum of

Table 4 The specifications of uncertain parameters

Parameters	Mean value	Standard deviation	Distribution
J (kg m^2)	10	2	Normal
U_m (N m)	1	0.2	Normal
M_d (N m)	0.02	0.02	Uniform
T_d (s)	0.02	0.01	Normal

Table 5 The obtained gains of controller for traditional and robust optimization

Optimization	Uncertainty	K_P (N m/rad)	K_D (N m s/rad)	K_I (N m/rad)	L (rad/N m)
Traditional	–	107.64	75.33	48.75	3.36
Robust	U_{m} (N m)	99.89	77.12	43.07	18.78
Robust	$J\left(\mathrm{kg\,m^2}\right)$	119.98	94.67	49.36	2.32
Robust	M_d (N m)	108.99	99.54	38.53	12.67
Robust	T_d (s)	111.55	90.23	37.3	24.19
Robust	U_m, J, M_d, T_d	108.83	97.32	38.38	24.92

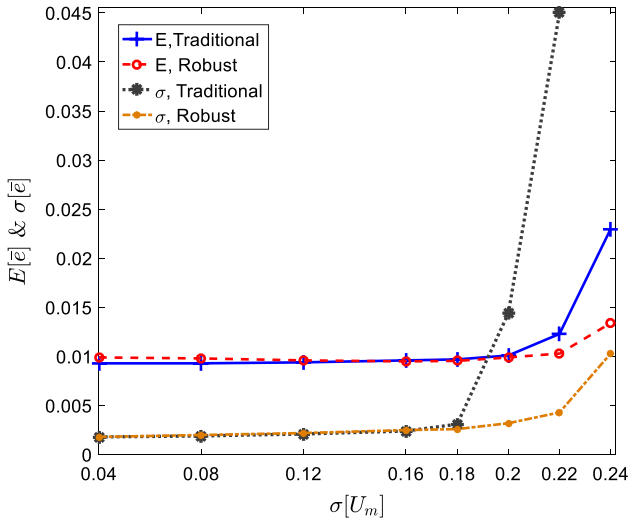

Fig. 8 Expected value and standard deviation of $\bar{e}$ versus uncertainty in U_m

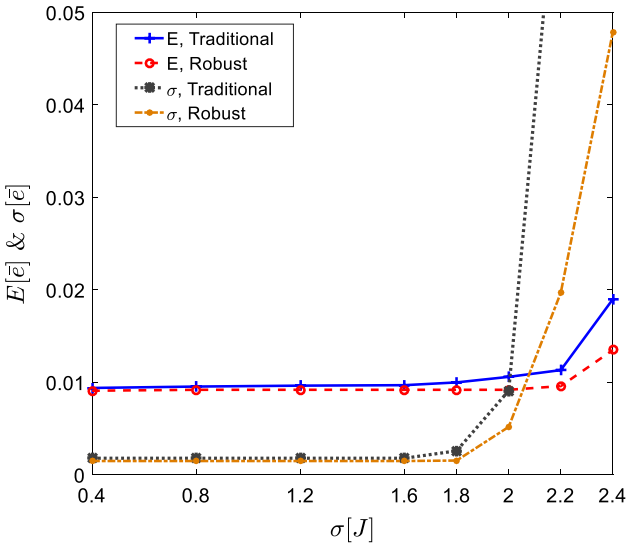

Fig. 9 Expected value and standard deviation of $\bar{e}$ versus uncertainty in J

the absolute value of the quasi-normalized pointing error in interval $[10\ t_f]$ is ≤ 0.1. The objective function (ϕ) is the weighted combination of the expected value and standard deviation of $\bar{e}$. The penalty function is added to ϕ when the constraint is violated. In RO algorithm, each run is repeated 500 times, and then the expected value and standard deviation of the original objective function are evaluated.

First, the controller gains are obtained for each parameter uncertainty when $u_{\mathrm{off}}/u_{\mathrm{on}} = 0.5$ and $\Theta_{\mathrm{ref}}/U_m = 15\,\mathrm{deg/N\,m}$. For the optimization, we set $\epsilon = 10^{-7}$, $P_\sigma/P_E = 200$, and Penalty = 100000. The obtained gains of controller are presented in Table 5 for each parameter uncertainty, and the last row shows the results for all of the uncertainties together.

The expected value and standard deviation of $\bar{e}$ are compared in Figs. 8, 9, 10, and 11 versus the value of the standard deviation of each uncertain parameter (as the input) for the traditional and robust optimization. Moreover, for simplicity, a same level of uncertainty is considered for the four mentioned uncertainties, as independent variables, and the results are plotted in Fig. 12; otherwise, the simulation results will be difficult to be illustrated. According to Figs. 8, 9, 10, 11, and 12, the expected value of $\bar{e}$ for the traditional optimization is better than the value for robust optimization

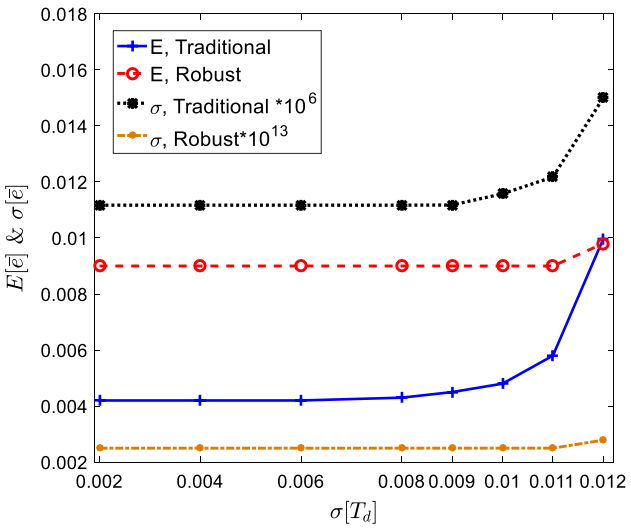

Fig. 10 Expected value and standard deviation of $\bar{e}$ versus uncertainty in T_d

when the standard deviation is small. Increasing the standard deviation to its nominal point, decreases the difference between the performances of the two optimization methods,

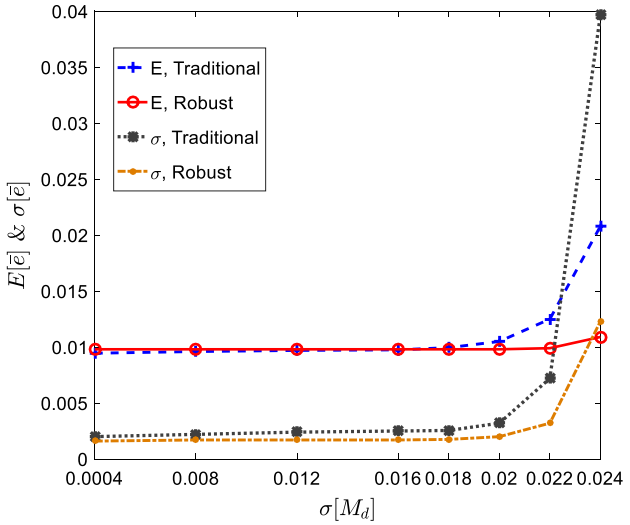

Fig. 11 Expected value and standard deviation of $\bar{e}$ versus uncertainty in M_d

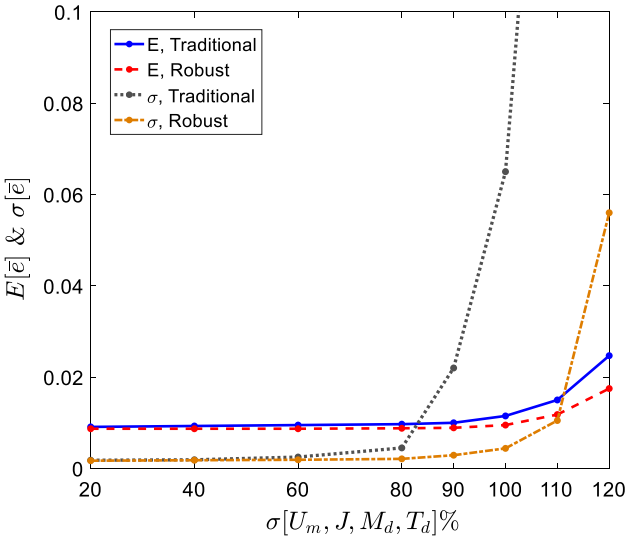

Fig. 12 Expected value and standard deviation of $\bar{e}$ versus four uncertainties in RO

but at a point lower than the nominal value of the standard deviation, the quasi-normalized pointing error of the traditional optimization increases significantly.

It should be noted that, for example, a standard deviation of thrust level uncertainty of 0.2 N m is set as the input (nominal) value of the RO as shown in Table 6, but the simulation results are carried out for the range of 0.04–0.22 N m which means an uncertainty of -80% to $+10\%$ for the nominal value of $\sigma(U_m)$. For other uncertain parameters, the nominal values of the standard deviations of the uncertainties are listed in Table 6 as mentioned before.

5 Reliability-based robust design optimization (RBRDO)

The controller parameters in the mentioned robust optimization are determined by the mean and standard deviation of the time average of the absolute value of the quasi-normalized pointing error. The disadvantage of the robust optimization is that the controller parameters are not determined by the number of the constraint violations. This is accomplished using reliability-based robust optimization as formulated according to Fig. 7 (including the dashed-line box) as follows [31]:

$$\begin{aligned}&\text{Find } (y)\\&\text{Minimizing } \phi(y,x) = P_E E[F(y,x)] + P_\sigma \sigma\left[F(y,x)\right] + \text{Penalty}(y,x)\\&\text{Subject to } \Gamma_i(y,x) = \text{CDF}_{G_i}^{-1}\left(1 - P_{f,i}^{\text{acc}}\right) \le 0,\ i = 1,\ldots I\\&y_j\text{min} \le y_j \le y_j\text{max}\end{aligned} \tag{10}$$

where Γ_i is the ith constraints function that obtained from the inverse cumulative distribution function (CDF) of G_i. The constraint function,Γ_i, guarantees the reliability $\geq (1 - P_{f,i}^{\text{acc}})$ in which $P_{f,i}^{\text{acc}}$ is the acceptable failure probability of a system as described in [30]. Other parameters are defined as same as the RO. The acceptable value of the probability of violating the constraint, $P_{f,i}^{\text{acc}}$, is chosen by the designer within the limited range related to the nature of a system. The formulation of the reliability-based robust optimization for the satellite attitude control illustrated in Fig. 3 is the same as Eq. (7) except the third line that is modified as follows [32]:

$$\text{Subject to } \Gamma_i(y,x) = \text{CDF}_{G_1}^{-1}\left(1 - P_{f,1}^{\text{acc}}\right) \le 0 \tag{11}$$

Table 6 The achieved controller gains in reliability-based robust optimization

Prescribed probability of failure (%)	K_P (N m/rad)	K_D (N m s/rad)	K_I (N m/rad)	L (rad/N m)
1	101.78	95.1	34.96	10.56
0.75	109.97	83.16	45.84	17.70
0.5	114.56	91.87	44.56	13.58

The problem constraint of optimization, G_1, i.e., the maximum of the absolute value of the quasi-normalized pointing error is chosen < 0.1 deg/N m. In other words, $\bar{e} \geq 0.1$ is chosen as the failure of the control system. The reliability-based robust design optimization has been performed for three different values of 0.5, 0.75 and 1% for acceptable probability of the failure under all uncertainties ($P_{f,i}^{\text{acc}} = 0.005, 0.0075, 0.01$). The obtained controller gains that achieved according to the flowchart of Fig. 7 are given in Table 6.

The probability of the failure is depicted in Fig. 13 versus the percentage value of the standard deviation of the uncertain parameters for different values of the acceptable probability of failure of 0.5%, 0.75%, and 1% as the input of RBRDO. These values are marked by dashed-line in the figure. The simulation results are shown for -100% to $+20\%$ uncertainty for the nominal value of the standard deviation of the thrust level, moment of inertia, external disturbance, and thruster delay, which means a range of standard deviation of (0–0.24, U_m), (0–2.4, J), (0–0.024,m_d), and (0–0.012, T_d) for the mentioned quasi-normalized uncertainties, respectively. According to Fig. 13, the probability of failure is lower than the input value for the acceptable probability of failure, P_f^{acc}, that we have set in RBRDO, as expected. Also, increasing the uncertainty in the standard deviation increases the probability of the failure. In addition, the robustness behavior of the expected value and standard deviation of $\bar{e}$ is compared with the traditional optimization in Fig. 14. Each point in Figs. 8, 9, 10, 11, 12, 13 and 14, shown by symbols, is obtained for 10,000 runs in Monte Carlo simulations using LHS sampling.

6 Discussion and results

In the previous sections, the behavior of an on–off satellite attitude control with obtained gains by traditional, robust and reliability-based optimization was studied. The behavior of the control response with traditional optimization is appropriate, but the performance decreases significantly in the presence of uncertainties, depending on levels of uncertainties. Robust optimization can increase the robustness of the system performance; however, the violation of constraints may be increased. The probability of failure can be chosen by the designer as an input for RBRDO. As a comparative study, the three types of optimizations are applied to the attitude control problem. A quantitative comparison in robustness and reliability is, here, made among the three types of the optimization techniques.

In order to study the robustness, the standard deviation of the time average of the absolute value of the quasi-normalized pointing error, i.e., the standard deviation of $\bar{e}$, can be evaluated in the presence of uncertainties. The standard deviation of $\bar{e}$ is plotted in Fig. 15 versus the uncertainty in the nominal values of the standard deviation of the parameters for the three optimization techniques. The standard deviation of $\bar{e}$ in the traditional optimization has the most variations in high uncertainties, whereas it has the least variations in the robust optimization as shown in Fig. 15. The standard deviation of $\bar{e}$ in RBRDO is somewhat between the two others. In addition, the expected value of $\bar{e}$ versus uncertainty in the nominal values of the standard deviation of the parameters is plotted in Fig. 16. As seen in the figure, in the traditional optimization, the expected value of $\bar{e}$, $E[\bar{e}]$, is the

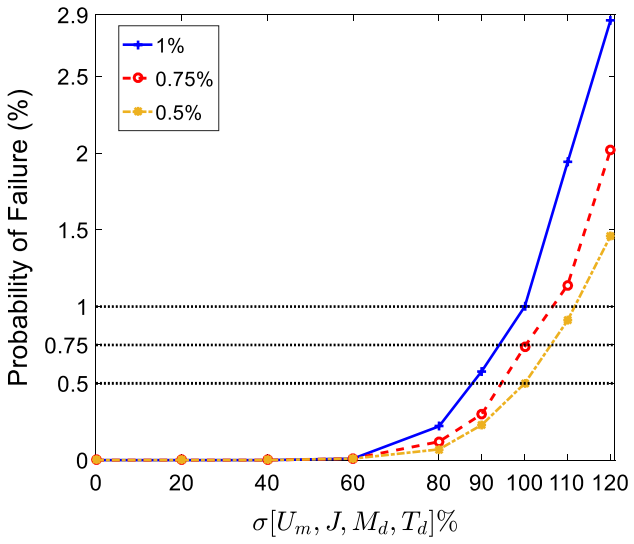

Fig. 13 Probability of failure versus percentage of the standard deviation of the uncertainties

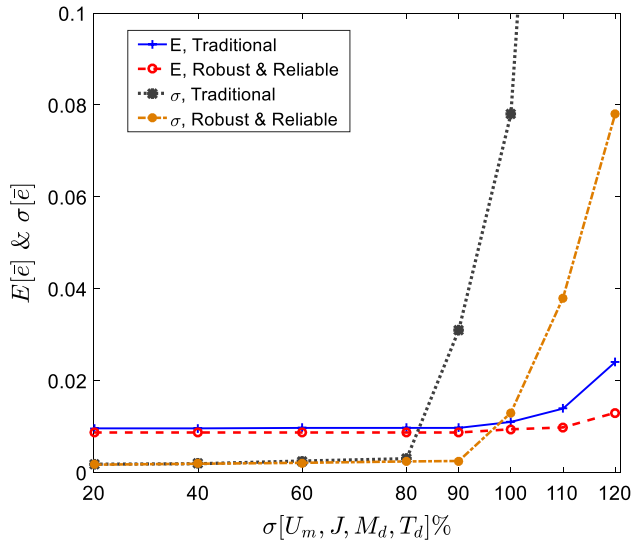

Fig. 14 Expected value and standard deviation of $\bar{e}$ versus percentage of the standard deviation of uncertainties

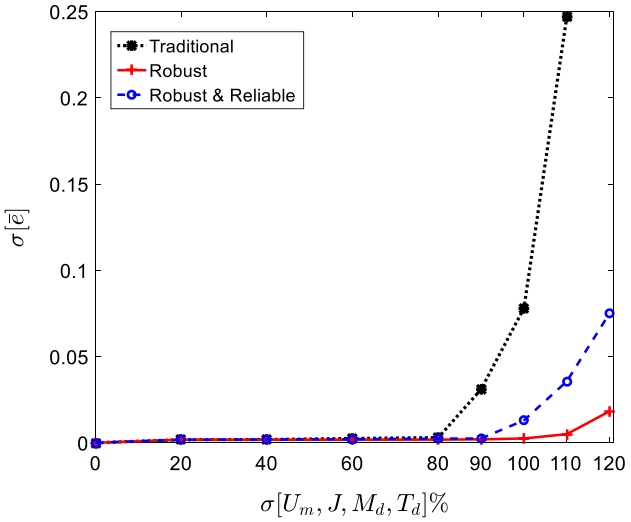

Fig. 15 Standard deviation of $\bar{e}$ versus percentage of standard deviation of uncertainties in traditional, RO, and RBRDO

least for low uncertainty, and it is the most for high uncertainty. Although $E[\bar{e}]$ of RO or RBRDO is larger than that of traditional optimization in low uncertainty, by increasing the percentage of uncertainty, $E[\bar{e}]$ of RO or RBRDO becomes (much) smaller than that of the traditional optimization, depending on the value of weight coefficient (P_σ/P_E). By decreasing the ratio of P_σ/P_E, the results for RO will be closer to that for traditional optimization.

To investigate the rates of failure of the attitude control, the probability of failure is depicted in Fig. 17 versus uncertainty in the nominal values of the standard deviation of the uncertain parameters for the three optimization techniques. For instance, the level of 0.5% is chosen as the criterion for probability of the failure, i.e., prescribed probability of failure in RBRDO method is given 0.005. The probability of failure increases by increasing the percentage of the uncertainty in all the three optimization techniques. In this case study, similar to the cases studied in [31], the probability of failure in RO is almost between traditional and RBRDO. According to Fig. 17, RBRDO provides $100 \times (1 - 0.004996) \simeq 99.5\%$ reliability for the given nominal values of the standard deviation of parameters (associated with the 0.5% of probability of failure), whereas the traditional and robust methods provide 99% and 99.18% of reliability, respectively. These values of reliability are obtained as 1 minus the probability of failure as shown in the figure. Therefore, it has been shown that using RBRDO it is possible to tune the probability of the failure for an on–off attitude control problem. Moreover, according to Figs. 15, 16, and 17, the results obtained from deterministic optimization are appropriate in low uncertainties, but RO is suggested in high uncertainties. RBDO is recommended to increase the reliability of the system in the presence of uncertainties.

Now, the effect of the ratio of the weight coefficients (P_σ/P_E) on the robustness and reliability of the system is studied. For this purpose, the standard deviation of $\bar{e}$ and the probability of failure are plotted in Fig. 18 versus P_σ/P_E for the nominal values of the standard deviations of the uncertain parameters as mentioned in Table 4 ($\theta_{\text{ref}} = 15\,\text{deg/N m}$, $m_d = 0.02$, and $T_d = 0.02$ s). As it can be seen in the figure, increasing P_σ/P_E decreases the overall standard deviation of $\bar{e}$, i.e., it increases the robustness of the system. According to Fig. 18, the results for

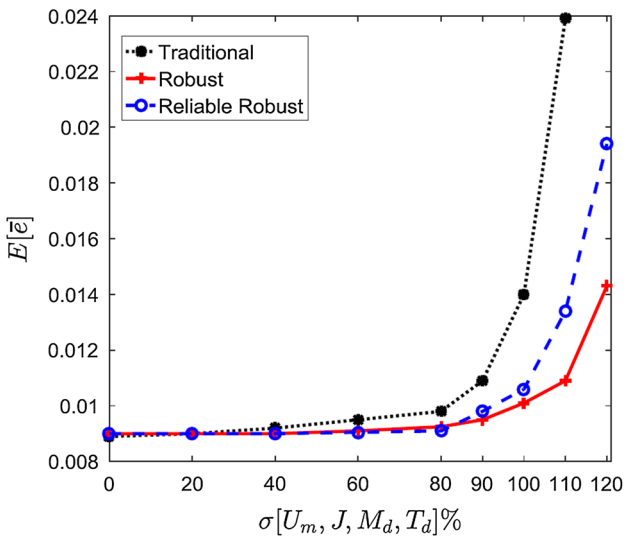

Fig. 16 Expected value of $\bar{e}$ versus percentage of standard deviation of uncertainties in traditional, RO, and RBRDO

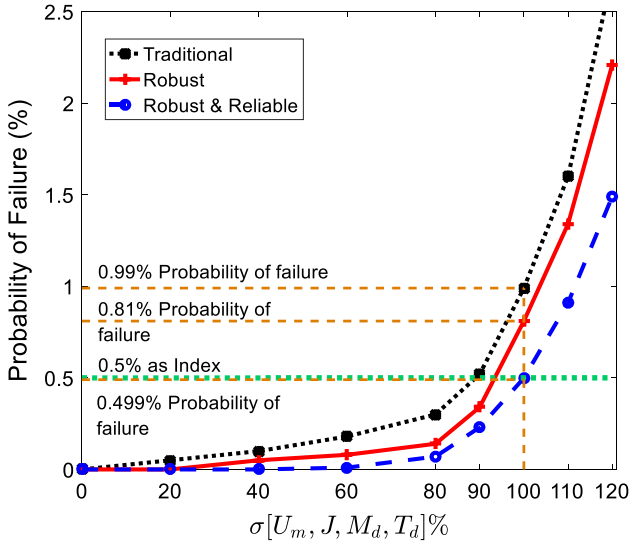

Fig. 17 Probability of failure versus percentage of standard deviation of uncertainties for the three optimization techniques

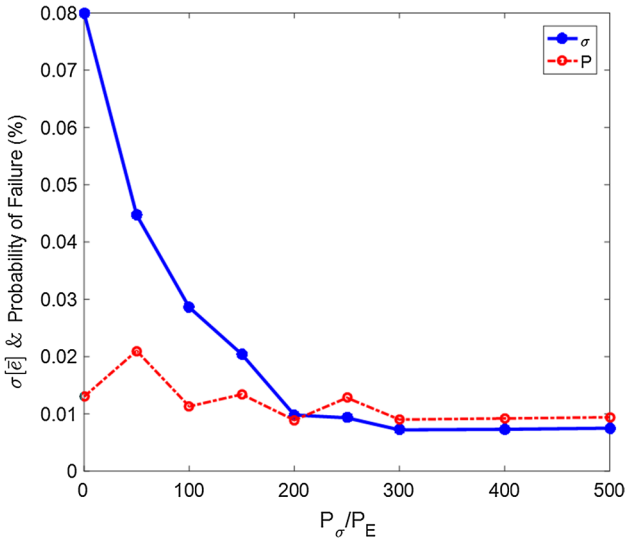

Fig. 18 The probability of failure and standard deviation of $\bar{e}$ versus P_σ/P_E

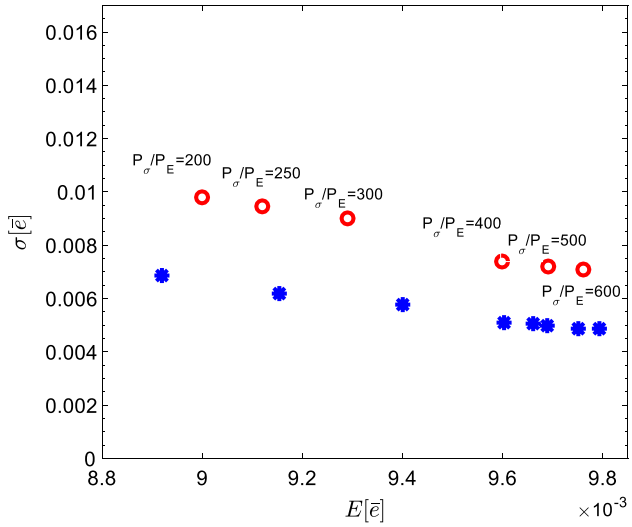

Fig. 19 The Pareto front of multi-objective optimization for on–off attitude control

RBRDO method, similar to those of RO, are relatively close to the results for the traditional optimization when the ratio of P_σ/P_E is small.

We expect a higher reliability for the system in RO method in comparison with the traditional optimization. This is because RO produces a narrow standard deviation of the error with respect to the traditional optimization as stated in the literature [35]. In addition, increasing P_σ/P_E increases the overall reliability of the system; however, it is limited by dynamics of the system and external disturbances. As seen in Fig. 18, the standard deviation of $\bar{e}$ and the reliability of the system, probably have an asymptotic behavior for very large values of P_σ/P_E.

An alternative approach is a multi-objective optimization, as described in the literature [27, 42] uses typically the Pareto front instead weight coefficient. For this purpose, two objective functions $(\sigma[\bar{e}], E[\bar{e}])$ are considered separately in a two-objective optimization using Pareto front technique as depicted in Fig. 19. As seen in the figure, there is a trade-off between the minimum values of $\sigma[\bar{e}]$ and $E[\bar{e}]$. Moreover, the results obtained from RO are shown in the figure for different values of weight coefficient P_σ/P_E. The obtained results from two-objective optimization agree with those of RO and may be considered as a verification of our results.

In this preliminary study, the assumed probability of failure has been shown to be achievable for a single-axis on–off attitude control for a specified reference input using RBRDO in the presence of external disturbance and model uncertainties. The controller gains can be determined for each specified reference input. However, it is suggested that an optimal rest-to-rest maneuver is implemented for the transient response. After the transient response, the present controller can be utilized for the pointing in the presence of external disturbance. For a (near-) zero input reference, the controller gains are available in [41]. The obtained results for the three-mentioned optimization methods are shown in Figs. 20, 21, 22.

In the analysis, the controller gains have been determined under some practical limitations, e.g., actuator lag and delay, actuator frequency limit, and external disturbances. If the thruster actuator is modeled by a transfer function and with no limit on its response frequency, the achieved pointing accuracy will not be valid, especially in the presence of external disturbances. This means an

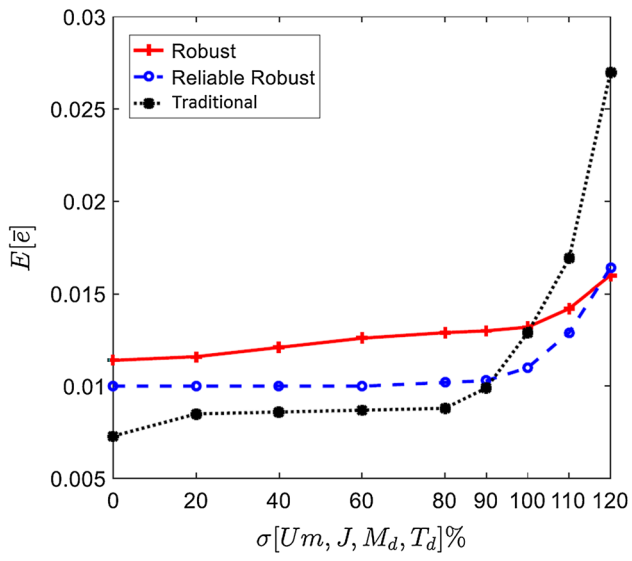

Fig. 20 Expected value of $\bar{e}$ versus percentage of standard deviation of uncertainties for the three optimization techniques

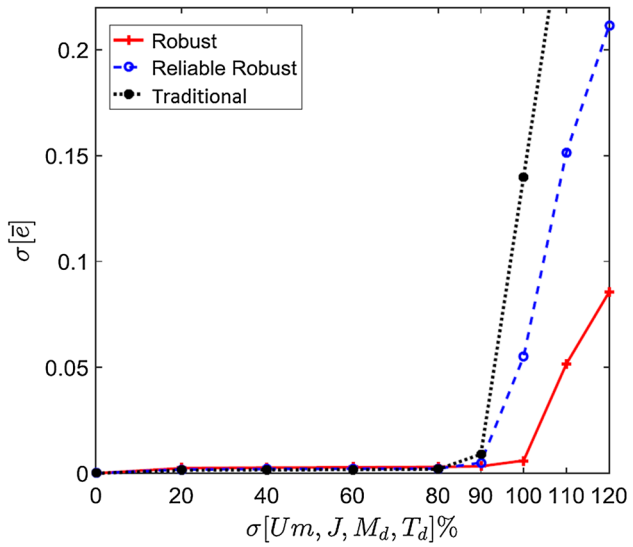

Fig. 21 Standard deviation of $\bar{e}$ versus percentage of standard deviation of uncertainties for the three optimization techniques

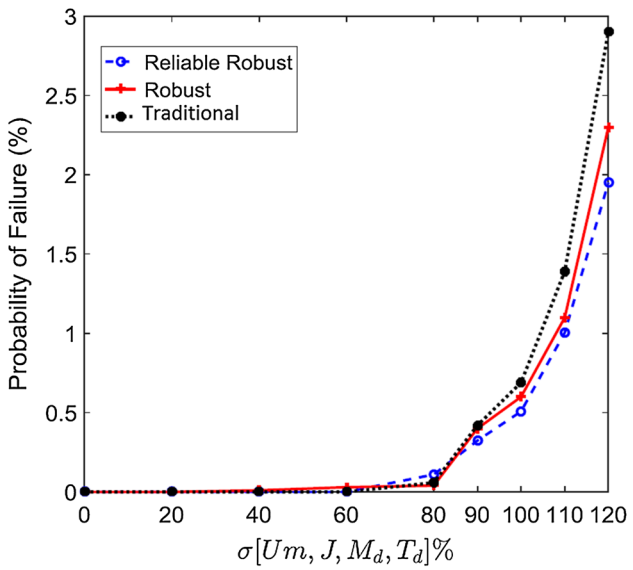

Fig. 22 Probability of failure versus percentage of standard deviation of uncertainties for the three optimization techniques

on–off thruster actuator converts into a continuous-type thruster when its input frequency is larger than its operational frequency.

As a future study, the sensor noise, three-axis control, and flexibility of spacecraft should be considered in the optimization problem for a practical design. For this case, the (quasi-) normalized form of equations is difficult to obtain; therefore, the optimization must be carried out for each set of the satellite characteristics and parameters.

Obviously, the optimization algorithm does not guarantee the stability of the control system. To investigate the stability of the control system in numerical optimization methods, it is suggested that engineering codes are developed to determine the stability regions under model uncertainty. In one approach, the failure points can be saved and analyzed for stability analysis for sufficiently long time. In the second approach, a stability criterion can be added to the optimization constraint for relatively short final time due to computational burden in the optimization algorithm. Since our sampling may not cover the stability boundaries for uncertain parameters, a safety factor can also be used for each corresponding standard deviation.

In each constraint violation, its time duration,T_v, is important in pointing mode. If the duration of each constraint violation is less than T_v, the result may be considered acceptable as a trade-off. For this case, the reliability of attitude control versus T_v is shown in Fig. 23 for the three values of prescribed probability of failure (0.5%, 0.75%, and 1%). The final time (t_f) is taken 40 s due to computational burden. As seen in the figure, the reliabilities are computed 99.46%, 99.93%, and 99.998% for $T_v = 0.1, 1$, and 10s respectively; when the prescribed value is 99%. If $T_v = 20$ s, the reliability will be 100% for the three-mentioned prescribed reliabilities when $t_f = 500$ s under given circumstances. This analysis is useful for exponentially unstable behavior, but the results must be checked for an oscillatory, unstable behavior.

In each run, number of violations from a specified T_v, is counted and denoted by N_i. If the probability of failure is 1%, we have 100 failures among 10,000 runs. For this case, we have N_1 to N_{100} ($i = 1, 2, \ldots 100$). The maximum and minimum values for N_i are plotted in Fig. 24. In this figure, as expected, the number of violations is decreased

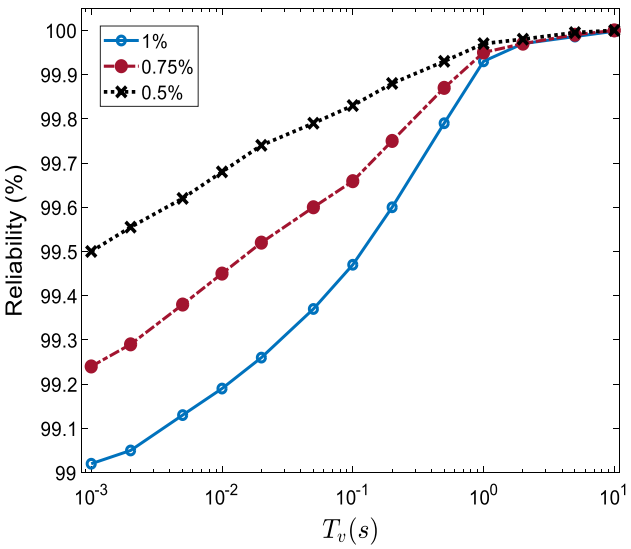

Fig. 23 Reliability of attitude control versus T_v

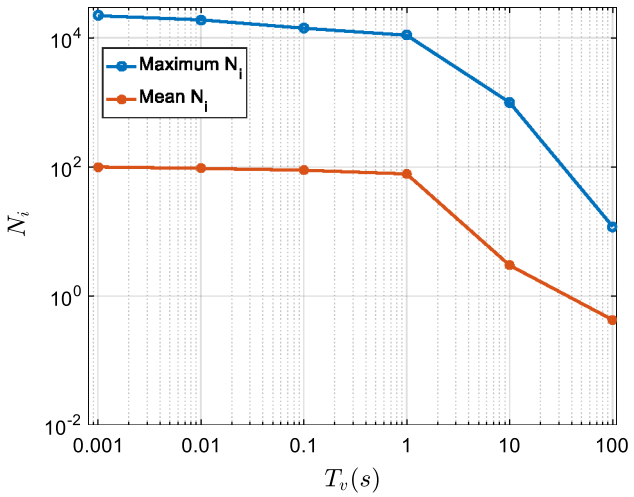

Fig. 24 Number of violations versus T_v

by increasing T_v until it vanishes. The frequency of isolated violations is computed by $N_i/t_f\left(t_f = 500\,\mathrm{s}\right)$.

As a modification, it is suggested that an allowable T_v and the frequency of isolated violations are considered as the constraints of a RBRDO in control applications. For this purpose, an inner loop will be added to the flowchart in Fig. 7 for the frequency constraint.

7 Conclusions

In this work, the robustness and reliability of a single-axis on–off attitude control for rigid satellites is enhanced using reliability-based robust design optimization in the presence of uncertainties. In this optimization technique, in addition to increase the robustness, a prescribed probability of failure is achievable. In other words, the controller gains are determined according to an acceptable level of probability of failure as the constraint of the optimization problem. Here, the observer-based anti-windup modified PI-D controller is utilized. The control signal is modulated by PWPF modulator and the commanded on–off signal to the thruster is limited to 50 Hz. The thruster is taken by a second-order transfer function with a delay of 0.02 s. The modified PI-D improves the pointing accuracy for an on–off attitude control under external disturbances and uncertainties.

In the analysis, the traditional, robust, and reliability-based robust design optimization techniques are carried out for the on–off attitude control problem and their performances are compared together. For this purpose, a level of -100% to $+20\%$ uncertainty is considered for nominal values of the standard deviation of the thrust level, moment of inertia, external disturbance, and the thruster delay.

Since quasi-normalized forms of equations have been utilized, the results are more applicable for satellites with different characteristics. In the optimization problem, the time average of the absolute value of quasi-normalized pointing error is chosen as the original objective function. The mean value and standard deviation of the original objective function and the probability of failure of attitude control are our problem criteria for the accuracy, robustness, and the reliability of the attitude control algorithm, respectively.

The simulation results show that a prescribed reliability for satellite pointing mode is achievable in the reliability-based robust design optimization, but in a range under limitation of our system dynamics, e.g., actuator lag and delay, actuator frequency limit, and external disturbances. The traditional optimization gives the best pointing accuracy with no uncertainty and even may be preferred in very low uncertainties. Increasing the level of uncertainty decreases the pointing accuracy significantly. For this case, the robust optimization gives an approximately flat behavior for the mean of the time average of absolute pointing error versus the level of uncertainties, with a small loss in accuracy, with respect to the traditional optimization. This accomplished with the use of a weighted combination of expected value and standard deviation of the time average of the absolute value of the quasi-normalized pointing error. In addition, a multi-objective optimization utilizing the Pareto front has been carried out as a verification of the obtained results for robust optimization. The robust optimization shrinks the distribution of probability of the performance and improves the reliability of the system, but a prescribed reliability cannot be achieved. Reliability-based robust design optimization satisfies the prescribed reliability in the presence of uncertainties, but under system limitations. This approach could increase the reliability of the satellite pointing mode in a practical situation.

References

1. Beyer HG, Sendhoff B (2007) Robust optimization—a comprehensive survey. Comput Methods Appl Mech Eng 196(33):3190–3218
2. Kobis E (2015) On robust optimization. J Optim Theory Appl 167(3):969–984
3. Krasopoulos CT, Beniakar ME, Kladas AG (2017) Robust optimization of high-speed PM motor design. IEEE Trans Magn 53(6):1–4
4. Yao W, Chen X, Luo W, Tooren M, Guo J (2011) Review of uncertainty-based multidisciplinary design optimization methods for aerospace vehicles. Prog Aerosp Sci 47(6):450–479
5. Diez M, Peri D, Fasano G, Campana EF (2010) Multidisciplinary robust optimization for ship design. In: 28th symposium on naval hydrodynamic, Pasadena, California, USA
6. Sternberg D, Chodas M, Jewison C, Jones M, De Weck O (2015) Multidisciplinary system design optimization of on orbit satellite assembly architectures. In: Aerospace conference. IEEE

7. Aoues Y, Chateauneuf A (2010) Benchmark study of numerical methods for reliability-based design optimization. Struct Multidiscip Optim 41(2):277–294
8. Taguchi G (1986) Introduction to quality engineering: designing quality into products and processes. American Supplier Institute, Dearborn
9. Mulvey JM, Vanderbei RJ, Zenios SA (1995) Robust optimization of large-scale systems. Oper Res 43(2):264–281
10. Chen W, Allen JK, Tsui KL, Mistree F (1996) A procedure for robust design: minimizing variations caused by noise factors and control factors. J Mech Des 118(4):478–485
11. Reis CJB, Manzanares-Filho N, de Lima AMG (2016) Robust optimization of turbomachinery cascades using inverse methods. J Braz Soc Mech Sci Eng 38(1):297
12. Malcolm SA, Zenios SA (1994) Robust optimization for power systems capacity expansion under uncertainty. J Oper Res Soc 45(9):1040–1049
13. Hajimiragha AH, Canizares CA, Fowler MW, Moazeni S, Elkamel A (2011) A robust optimization approach for planning the transition to plug-in hybrid electric vehicles. Trans Power Syst 26(4):2264–2274
14. Reis CJB, Manzanares-Filho N, Lima AMG (2019) Robust optimization of aerodynamic loadings for airfoil inverse designs. J Braz Soc Mech Sci Eng 41(1):207
15. Kerrigan EC, Maciejowski JM (2003) On robust optimization and the optimal control of constrained linear systems with bounded state disturbances. In: European Control Conference, pp 1453–1458
16. Lopez RH, Ritto TG, Sampaio R, de Cursi JES (2014) Optimization of a stochastic dynamical system. J Braz Soc Mech Sci Eng 36(2):257–264
17. Haas L, Steinbuch R (2016) Robust and reliable bionic optimization of nonlinear control problems. In: International conference on intelligent systems design and applications. Springer, pp 165–174
18. Bruni R, Celani F (2017) A robust optimization approach for magnetic spacecraft attitude stabilization. J Optim Theory Appl 173(3):994–1012
19. Bohlouri V, Jalali-Naini SH (2018) Robust optimization of satellite attitude control with thruster actuators based on combined objective function. J Space Sci Technol 10(4):55–66 **(in Persian)**
20. Bohlouri V, Ebrahimi M, Jalali-Naini SH (2017) Robust optimization of satellite attitude control system with on-off thruster under uncertainty. In: 2017 International Conference Mechanical, System and Control Engineering (ICMSC), pp 328–332
21. Bruni R, Celani F (2019) Combining global and local strategies to optimize parameters in magnetic spacecraft control via attitude feedback. J Optim Theory Appl 181(3):997–1014
22. Du X, Sudjianto A, Chen W (2004) An integrated framework for optimization under uncertainty using inverse reliability strategy. J Mech Des 126(4):562–570
23. Motta RDS, Afonso SM (2016) An efficient procedure for structural reliability-based robust design optimization. Struct Multidiscip Optim 54(3):511–530
24. Dizangian B, Ghasemi MR (2016) A fast decoupled reliability-based design optimization of structures using B-spline interpolation curves. J Braz Soc Mech Sci Eng 38(6):1817–1829
25. Dizangian B, Ghasemi MR (2016) A fast decoupled reliability-based design optimization of structures using B-spline interpolation curves. J Braz Soc Mech Sci Eng 38(6):1817–1829
26. Wang W, Wu J (1998) Reliability-based robust design. In: 39th AIAA/ASME/ASCE/AHS/ASC Structures, Structural Dynamics, and Materials Conference and Exhibit, p 2052
27. Gu X, Sun G, Li G, Mao L, Li Q (2013) A comparative study on multi-objective reliable and robust optimization for crashworthiness design of vehicle structure. Struct Multidiscip Optim 48(3):669–684
28. Chung G, Lansey K, Bayraksan G (2009) Reliable water supply system design under uncertainty. Environ Model Softw 24(4):449–462
29. Paiva RM, Crawford C, Suleman A (2014) Robust and reliability-based design optimization framework for wing design. AIAA J 52(4):711–724
30. Su CQ, Li LX, Zhang YM (2012) Reliability-based robust optimization design for rubbing rotor system. Appl Mech Mater 105(1):1100–1104
31. Venanzi I, Materazzi AL, Lerimonti L (2015) Robust and reliable optimization of wind-excited cable-stayed masts. J Wind Eng Ind Aerodyn 147(1):368–379
32. Budianto IA, Olds JR (2004) Design and deployment of a satellite constellation using collaborative optimization. J Spacecr Rockets 41(6):956–963
33. Jafarsalehi A, Fazeley HR, Mirshams M (2016) Conceptual remote sensing satellite design optimization under uncertainty. Aerosp Sci Technol 55(1):377–391
34. Guo SX (2014) Robust reliability based optimal design of H∞ control of parametric uncertain systems. J Dyn Syst Meas Control 136(2):024504
35. Kumar CA, Rajeshwaran S, Ganapathy K (2018) Robust proportional integral derivative controller design for various processes using novel hybrid metaheuristic algorithms. J Dyn Syst Meas Control 140(8):81006
36. Song G, Buck NV, Agrawal BN (1999) Spacecraft vibration reduction using pulse-width pulse-frequency modulated input shaper. J Guid Control Dyn 22(3):433–440
37. Kim J, Crassidis JL (1998) A comparative study of sliding mode control and time optimal control. In: AIAA/AAS Astrodynamics Specialist Conference and Exhibit, USA
38. Åström KJ, Hägglund T (1995) PID controllers: theory, design, and tuning. Instrument Society of America, Research Triangle Park
39. Bohlouri V, Jalali-Naini SH (2018) Spacecraft attitude control using model-based disturbance feedback control strategy. J Braz Soc Mech Sci Eng 40(12):557
40. Wang Z, Su Y, Zhang L (2018) A new nonsingular terminal sliding mode control for rigid spacecraft attitude tracking. J Dyn Syst Meas Control 140(5):51006
41. Bohlouri V, Jalali-Naini SH (2018) Reliable robust versus reliable optimization for attitude control under uncertainties. In: 17th International Conference of Iranian Aerospace Society, Tehran, Iran
42. Santos WGD, Rocco EM, Boge T, Benninghoff H, Rems F (2015) Multi-objective optimization applied to real-time command problem of spacecraft thrusters. J Spacecr Rockets 52(5):1407–1416